Classical cross section for chaotic potential scattering



1989 J. Phys. A: Math. Gen. 22 2925

(http://iopscience.iop.org/0305-4470/22/15/011)

J. Phys. A: Math. Gen. 22 (1989) 2925-2938. Printed in the UK

# Classical cross section for chaotic potential scattering

C Jung and S Pott

Fachbereich Physik, Universität Bremen, 2800 Bremen, Federal Republic of Germany

Received 8 December 1988

**Abstract.** We investigate the differential cross section for a scattering system for which the existence of topological chaos in the phase space has already been shown in a previous paper. The most important result is the arrangement of an infinity of rainbow singularities into a fractal structure with a binary organisation. Its scaling behaviour is given by the eigenvalues of some periodic orbits. We discuss to what extent these results are typical for any chaotic scattering system.

## 1. Introduction

In recent years much work has been done on chaos in bound classical Hamiltonian systems. Meanwhile it is well known how chaos shows up in these systems, and powerful methods have been developed to investigate its behaviour. In contrast, the understanding of chaos in classical scattering systems is less complete.

From the mathematical point of view it has been shown that topological chaos can exist on non-compact energy surfaces due to the interplay of homoclinic and heteroclinic connections of unstable periodic bound orbits (Churchill *et al* 1979). For nearly twenty years there have been numerical observations of complicated behaviour in classical models for inelastic molecular scattering (Rankin and Miller 1971, Gottdiener 1975, Fitz and Brumer 1979, Agmon 1982, Schlier 1983, Noid *et al* 1986, Skodje and Davis 1988). More recently, chaos has been found in satellite encounters (Petit and Henon 1986), vortex dynamics (Eckhardt 1988a, Eckhardt and Aref 1988), soliton scattering (Campbell *et al* 1986) and potential scattering (Eckhardt and Jung 1986, Jung and Scholz 1987, 1988, Troll and Smilansky 1988). (See also the review article by Eckhardt (1988b) and references therein.)

In these systems the final asymptote has been observed as a function of the initial asymptote and it has been found to contain discontinuities on a fractal set. Accordingly, the best definition for scattering chaos, known so far, is the following. A scattering system is chaotic if the deflection function or any other convenient property of the final asymptote is discontinuous on a fractal subset of its domain, which is the set of all incoming asymptotes. In most of the work mentioned above the scattering cross sections have not been considered and it is not known whether they contain any specific effects coming from the topological chaos in the flow. In some of the molecular systems the probability for excitation or reaction has been studied. However, these are cross sections already integrated over the angles and possibly over some other final quantities. And, even if the differential cross section shows chaotic effects, they might have been averaged out during the integration.

0305-4470/89/152925+14$02.50  

We suggest that chaotic effects in the cross section be identified first in the differential cross section. Therefore the purpose of the present paper is the following. In the differential cross section of a chaotic scattering system we look for structures which arise from the topological chaos in the flow. To keep things as simple as possible, we start with the simplest type of scattering system which can exhibit chaos at all, namely potential scattering in a two-dimensional position space. As an example we take the potential

$$V(x, y) = \exp[-(x+\sqrt{2})^2 - y^2] + \exp[-(x-1/\sqrt{2})^2 - (y+\sqrt{3/2})^2 + \exp[-(x-1/\sqrt{2})^2 - (y-\sqrt{3/2})^2] \tag{1}$$

where $x$, $y$ are the cartesian coordinates in position space. In Jung and Scholz (1987, hereafter referred to as JS) it has been demonstrated that there is topological chaos in the flow of this system. In particular it has been shown that the deflection function, as a function of the impact parameter, shows discontinuities on a Cantor set, which is qualitatively the same as the standard $\frac{2}{3}$ Cantor set. This particular type of fractal set allows for a simple binary signature for the intervals of continuity in between the points of the Cantor set itself.

Accordingly, we build up the complete cross section as a sum over the contributions from these various open intervals. (Note: the Cantor set itself has measure zero. Therefore it does not contribute to the cross section.) The possibility for such a summation suggests the way in which the paper is organised. In § 2 the contribution to the cross section from one particular interval of continuity of the deflection function is given. In § 3 we explain that all intervals give contributions of similar structure, the only essential difference being the exact angular position of the rainbow singularities. These singularities from all the various intervals are arranged in the form of a binarily organised fractal structure, which will be presented in more detail in § 4. Section 5 contains final remarks, and in particular a discussion as to what extent our results are typical for other chaotic scattering systems.

## 2. One interval of continuity

The straight line asymptotes of the system are labelled by the three quantities $E$, $\alpha$, $b$. $E$ is the energy, in the asymptotic region $E = (p_x^2 + p_y^2)/2$, where $p_x$, $p_y$ are the momenta conjugate to $x$, $y$. $\alpha$ is the direction of the incoming momentum, $\alpha = \tan^{-1}(p_y/p_x)$. $b$ is the incoming impact parameter, $b = (xp_y - yp_x)/(p_x^2 + p^2)^{1/2}$. The scattering angle $\theta$ is the difference between the direction of the outgoing momentum and the direction of the incoming momentum. All angles are defined up to shifts by an integer multiple of $2\pi$.

The computation of the cross section is done like this. We fix the energy $E$ and the incoming direction $\alpha$ and take the scattering angle $\theta$ as a function of the incoming impact parameter $b$. We determine all values $b_j$ of the impact parameter which lead to some particular scattering angle $\theta_0$, i.e. we look for all solutions of $\theta(b) = \theta_0$. For each solution $b_j$ the quantity $(\mathrm{d}\theta/\mathrm{d}b)(b_j)$ is formed and the value of the cross section for the angle value $\theta_0$ is summed up as

$$\frac{\mathrm{d}\sigma}{\mathrm{d}\theta}(\theta_0) = \sum_j \left( \left| \frac{\mathrm{d}\theta}{\mathrm{d}b}(b_j) \right| \right)^{-1}. \tag{2}$$

Because of this additivity we now look at the contribution coming from one interval of continuity and delay the summation over all intervals to the next section.

Let us choose the values $E = 0.6$ and $\alpha = \pi$, as most of the plots in JS have been made for these values. In figure 1 we show the scattering angle as a function of the impact parameter. We observe a few $b$ values at which $\theta$ changes rapidly and we find intervals of continuity in between in which $\theta$ is a smooth function. The two intervals of generation 1 are labelled by $L$ and $R$ in figure 1. Under magnification (shown in figures 3 and 4 in JS) new smaller intervals of continuity appear close to the boundaries of the intervals $L$ and $R$. These gaps of generation 2 are denoted by sequences of two letters. The first letter is the same as the signature of the nearby gap of generation 1. The second letter becomes $L$ or $R$ according to whether the new interval lies to the left or right of the parent gap of generation 1. We continue this scheme by induction for those new intervals which appear close to the boundaries of the intervals of the previous generation under repeated magnification of the $b$ axis (for more details see JS).

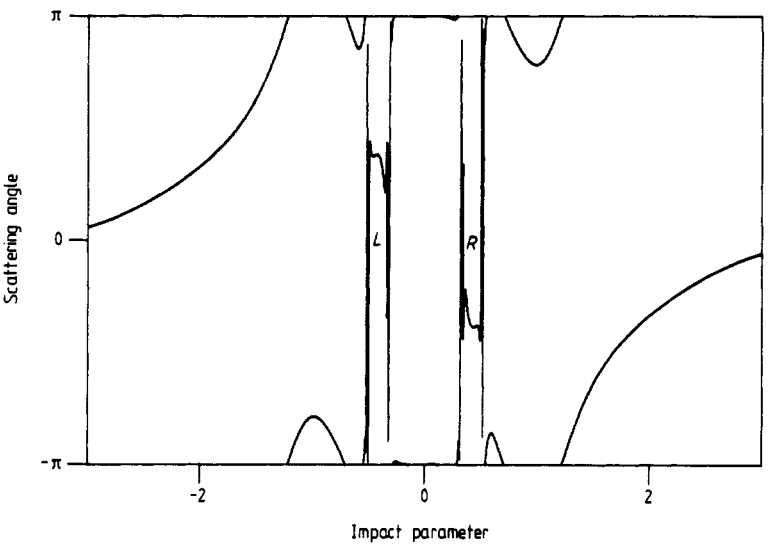


**Figure 1.** Scattering angle as a function of impact parameter for energy $E = 0.6$ and incoming direction $\alpha = \pi$.

In this section we choose the particular interval $R$ which corresponds to $b \in (b_{R-}, b_{R+}) = (0.341\,06\ldots, 0.497\,33\ldots)$. This interval gives the most important contribution for angle values close to $\theta = 5\pi/3$. In figure 1 the behaviour close to the boundaries of the interval $R$ is not well resolved. Therefore figure 2 shows the deflection function of the interval $R$ again, this time as a function of the logarithmically transformed impact parameter:

$$B = \ln[(b - b_{R-})/(b_{R+} - b)]/\ln \mu \tag{3}$$

where $\mu$ is the eigenvalue of the oscillating periodic orbit $\gamma$ on the saddles of the potential (in JS a plot of this orbit is shown in figure 7($a$)). At energy $E = 0.6$ its value is close to 107. By transformation (3) the interval $(b_{R-}, b_{R+})$ is mapped one-to-one onto $(-\infty, +\infty)$. For $B \to +\infty$ the deflection function as a function of $B$ can be fitted

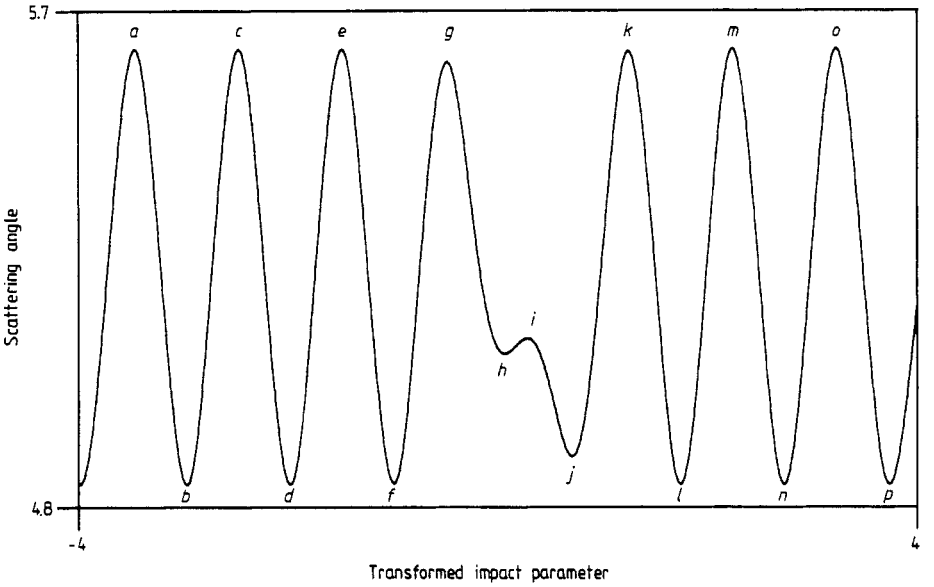


**Figure 2.** Scattering angle $\theta$ as a function of the logarithmically transformed impact parameter $B$ of (3). For comparison with figures 3 and 7 the relative extrema are labelled.

quite well by the closed form expression

$$\theta(B) \to 5\pi/3 + \theta_M[1 - c_{R+}\exp(-B\ln\mu)]\sin(2\pi B + \varphi_{R+}) \tag{4a}$$

and in the same way for $B \to -\infty$ by

$$\theta(B) \to 5\pi/3 + \theta_M[1 - c_{R-}\exp(B\ln\mu)]\sin(2\pi B + \varphi_{R-}) \tag{4b}$$

where $\theta_M = 0.394\,875\ldots$.

The approximate periodicity of $\theta(B)$ for $B \to \pm\infty$ can be understood as follows. If $b$ is close to the boundary of the interval of continuity, then the position space trajectory performs oscillations on the saddle before it leaves the potential region. If the value of $b$ comes closer to $b_{R-}$ or $b_{R+}$ by a factor $\mu$, then the position space trajectory spends one more period along $\gamma$. Accordingly, the factor $1/\ln\mu$ in (3), together with the sine function in (4), ensures that $\theta(B)$ assumes the same value. For $b$ values in between, all angle values are obtained which can be reached by trajectories leaving the periodic orbit $\gamma$ close to its unstable manifold.

To understand the slight deviation from periodicity note that, when the scattering trajectory moves along $\gamma$ for some additional turns, more energy is put into the transverse motion, and the deviation of the angle value from its middle value $5\pi/3$ can become greater. In the extreme case of $b \to b_{R\pm}$ the amplitude of the oscillations of the scattering angle converges to $\theta_M$. This approach of the oscillations to their maximal amplitude is adequately described by the factor $[1 - c_{R\pm}\exp(\mp B\ln\mu)]$ in (4). The behaviour of $\theta(B)$ close to $B = 0$ is determined by the particular shape of the potential and by the particular value of the energy, and we did not find any simple analytical fit for it.

Figure 3 shows the contribution of the interval $R$ to the cross section. Each relative extremum of $\theta(b)$ gives one rainbow singularity in the cross section. We have marked

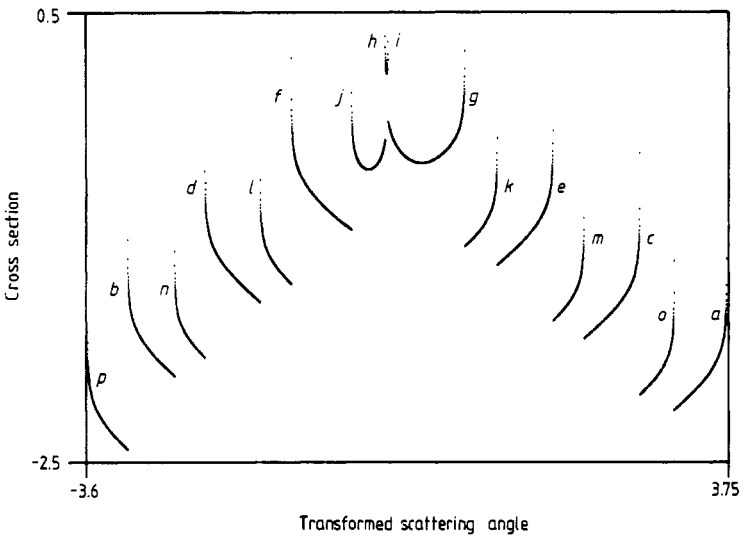


**Figure 3.** Contribution of the interval $R$ to the differential cross section. The logarithm of the cross section is plotted as a function of the logarithmically transformed scattering angle of (5). The rainbow singularities of the cross section are labelled to indicate the one-to-one correspondence between the rainbows and the extrema of the deflection function shown in figure 2.

the extrema in figure 2 and the corresponding singularities in figure 3 by the same letters. In figure 3 we have chosen logarithmic scales on both axes in order to demonstrate the simple scaling properties of the system. The abscissa gives the transformed scattering angle:

$$\psi(\theta) = \ln[(\theta - 5\pi/3 + \theta_M)(5\pi/3 + \theta_M - \theta)^{-1}]/\ln \mu. \tag{5}$$

In these coordinates the angular distance between any rainbow and its successor (the one coming from the neighbouring extremum in figure 2) becomes 1 in the limit $B \to \infty$. Compare, e.g., the distance between $p$ and $n$, or $b$ and $d$, or $m$ and $o$, etc. Along the ordinate the quantity $\ln(\mathrm{d}\sigma/\mathrm{d}\theta)/\ln \mu$ is plotted. We notice that each branch is shifted vertically by approximately $\frac{1}{2}$, as compared with its successor. The reason is as follows. Close to a maximum of $\theta(b)$ at $b = b_n$ with angle value $\theta = \theta_n$ we approximate $\theta(b) = \theta_n - A\,(b - b_n)^2/2$ and find

$$\left|\frac{\mathrm{d}\theta}{\mathrm{d}b}(b_n)\right| = |A(b - b_n)| = [2(\theta_n - \theta)A]^{1/2}. \tag{6a}$$

Close to the neighbouring maximum at $b_{n+1}$ with angle value $\theta_{n+1}$ we approximate $\theta(b) = \theta_{n+1} - A\mu^2\,(b - b_{n+1})^2/2$ and find

$$\left|\frac{\mathrm{d}\theta}{\mathrm{d}b}(b_{n+1})\right| = |A\mu^2(b - b_{n+1})| = \mu[2(\theta_{n+1} - \theta)A]^{1/2} \tag{6b}$$

where, according to (3) and (4), the $b_n$ and $\theta_n$ scale as $b_{R+} - b_n \approx \mu(b_{R+} - b_{n+1})$ and $5\pi/3 + \theta_M - \theta_n \approx \mu(5\pi/3 + \theta_M - \theta_{n+1})$. Let $\psi_n = \psi(\theta_n)$ and $\psi_{n+1} = \psi(\theta_{n+1})$ be the transformed scattering angles at $\theta_n$, $\theta_{n+1}$. We compare the cross section at two angle values $\bar{\psi}$ and $\tilde{\psi}$ which lie close to $\psi_n$ and $\psi_{n+1}$, respectively, such that

$$\psi_n - \bar{\psi} = \psi_{n+1} - \tilde{\psi} \ll 1. \tag{7}$$

$\bar{\psi}$ and $\tilde{\psi}$ correspond to the values $\bar{\theta}$ and $\tilde{\theta}$ of the original angle $\theta$. Equation (5) and (7) imply $\theta_n - \bar{\theta} \approx \mu\ (\theta_{n+1} - \tilde{\theta})$. Inserting this into (6*a*) and (6*b*) leads to

$$\left|\frac{d\theta}{db}(\tilde{\theta})\right| = \mu[2A(\theta_{n+1} - \tilde{\theta})]^{1/2} = [2A\mu(\theta_n - \bar{\theta})]^{1/2} = \mu^{1/2}\left|\frac{d\theta}{db}(\bar{\theta})\right|.$$

Accordingly, for the ratio between the contributions to the cross section coming from the vicinities of the two maxima we obtain

$$\frac{d\sigma}{d\theta}(\tilde{\theta}) = \mu^{-1/2}\frac{d\sigma}{d\theta}(\bar{\theta})$$

or

$$\ln\frac{d\sigma}{d\theta}(\tilde{\theta})/\ln\mu = \ln\frac{d\sigma}{d\theta}(\bar{\theta})/\ln\mu - \tfrac{1}{2}.$$

Analogous considerations hold for the minima.

At the energy $E = 0.6$ the two extrema of $\theta(b)$ in the middle of the interval, labelled *h* and *i* in figure 2, are not separated very much in their $\theta$ values. This causes a corresponding double singularity in the cross section which comes close to a cubic rainbow. It forms the most prominent structure in the cross section.

## 3. Contributions from all intervals

The next step is to demonstrate that all intervals of continuity give similar contributions to the cross section. This can be done as follows. We take an interval of continuity of the impact parameter line (at fixed incoming angle) and transport it by the flow through the potential until it reaches the region of outgoing asymptotes. There we make a plot of the values of the scattering angle $\theta$ and the outgoing angular momentum $L$ (which is equivalent to the outgoing impact parameter). Thereby any interval of continuity of the incoming impact parameter line is mapped onto a continuous curve in the $\theta/L$ plane. Figure 4 shows the results for the three intervals *R*, *LL*, *LR*. All other intervals that lead to $\theta$ values around $5\pi/3$, give spiral lines which run alongside these three lines in qualitatively the same manner. The only difference between these various spirals is a shift of the middle structure which produces the almost cubic rainbow structure in the cross section. The outer boundary line of the spirals is the intersection between the asymptotic $\theta/L$ plane and the branch of the unstable manifold $W^u$ of $\gamma$, which leaves the potential directly (compare figure 6 in JS). The image of any *b* interval of continuity spirals towards this boundary line in such a way that, for each complete turn, the distance from the boundary decreases by a factor $\mu$. If a position space trajectory makes one more turn along $\gamma$, then it lies closer to the unstable manifold $W^u$ by a factor $\mu$. Spirals from different intervals are not allowed to intersect each other. Therefore, all spirals must converge to the boundary line by the same rate. This universal scaling behaviour for all intervals originates from the fact that the boundary points of the various intervals considered here lie on the stable manifold of the same periodic saddle trajectory.

In this sense the scaling behaviour of all intervals is the same as the one described in § 2 for the interval *R*, and the structure of the analytical fit of (4) holds for any interval. For the various intervals we only have to insert other boundary values $b_+$, $b_-$ for the impact parameter transformation in (3) and other constants $c_+$, $c_-$, $\varphi_+$, $\varphi_-$ in (4). As an example, in figures 5 and 6 we show the deflection function of the

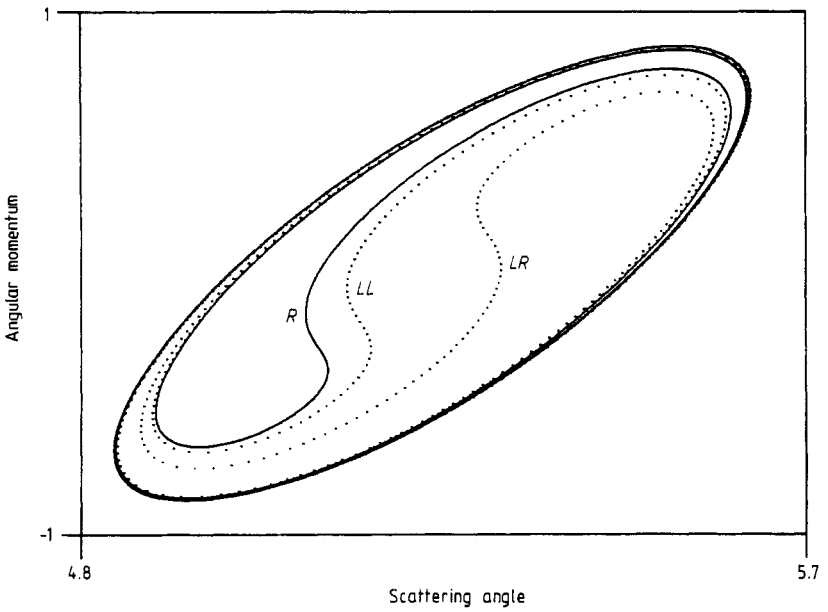


**Figure 4.** Intersection of the trajectories coming from intervals $R$, $LL$, $LR$ with the asymptotic plane of scattering angle $\theta$ and angular momentum $L$.

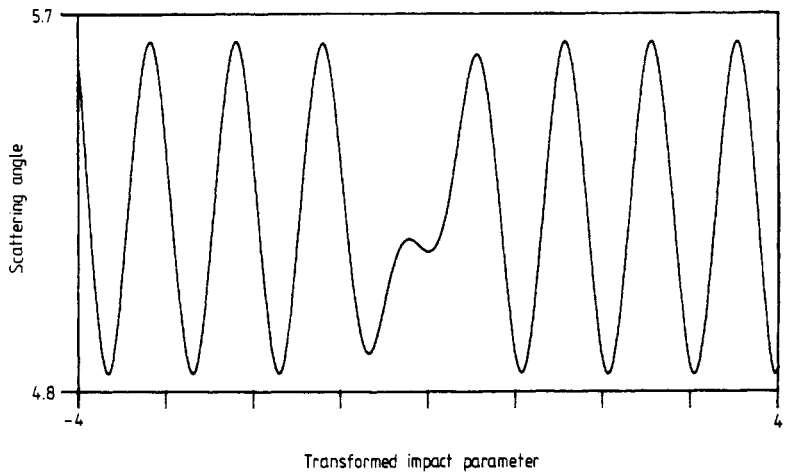


**Figure 5.** Scattering angle $\theta$ as a function of the logarithmically transformed impact parameter in the interval $LL$.

intervals $LL$ and $LR$ in the corresponding transformed coordinates, where $b_{LL-} = -0.513\,55\ldots$, $b_{LL+} = -0.502\,80\ldots$, $b_{LR-} = -0.338\,31\ldots$, $b_{LR+} = -0.321\,22\ldots$.

In order to show the convergence of the spirals to the boundary line and the scaling behaviour in better resolution, we show parts of the spirals from figure 4 again in figure 7, this time on a logarithmic scale. The exact transformation of the coordinates is this. In the $\theta/L$ plane we introduce polar coordinates $(r, \varphi)$ with the origin at $\theta = 5\pi/3$, $L = 0$. The boundary line of $W^u$ is given by a closed curve $r = f(\varphi)$, $\varphi \in (0, 2\pi]$. The map from the old coordinates $(r, \varphi)$ to new polar coordinates $(R, \Phi)$

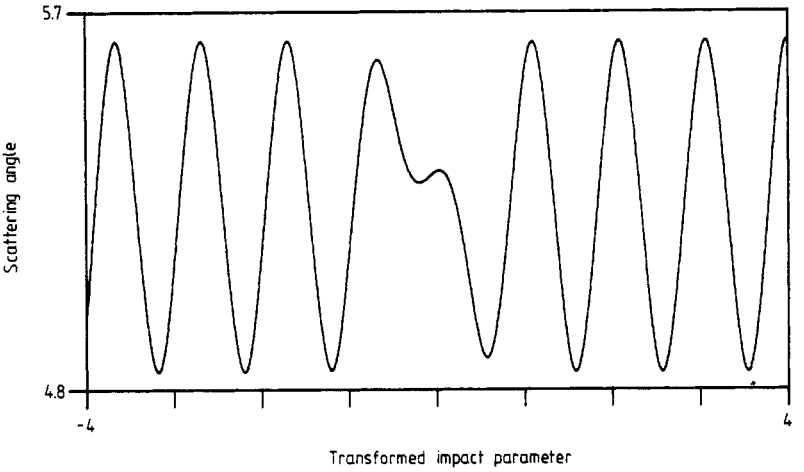


**Figure 6.** Scattering angle $\theta$ as a function of the logarithmically transformed impact parameter in the interval $LR$.

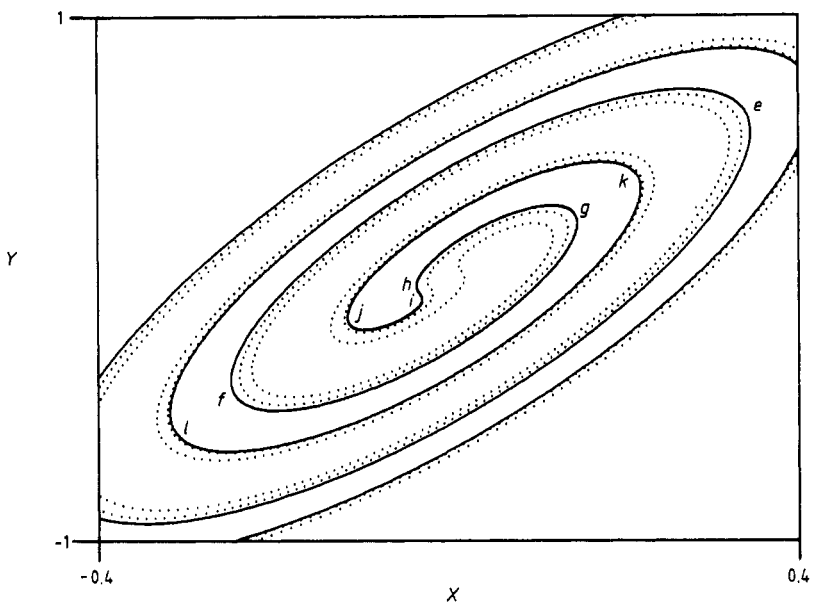


**Figure 7.** The same as figure 4 in logarithmically transformed coordinates to (8).

is given by

$$\Phi(r, \varphi) = \varphi \tag{8a}$$

$$R(r, \varphi) = f(\varphi) \tanh^{-1}(r/f(\varphi))/\ln \mu. \tag{8b}$$

The new polar coordinates are converted into new cartesian coordinates $X$, $Y$ and plotted in figure 7. Some of the extremal values of the angle $\theta$ along the spiral corresponding to the interval $R$ are labelled by letters which match the letters of figures 2 and 3.

There is a natural one-to-one correspondence between the extremal angle values of interval $R$ and the extremal angle values of the other intervals. Therefore, all

intervals create qualitatively the same rainbow structures in their contributions to the cross section. There are only two differences between the various contributions. First, the exact values of the rainbow angles are slightly shifted according to the shift of the spirals in figures 4 and 7. Second, the total weight of the contribution of any interval is proportional to its length, i.e. proportional to the amount of incoming flux which falls in this interval.

Figure 8 presents the cross section of the combined contributions from the intervals *R*, *LL*, *LR*, this time as a function of the untransformed scattering angle $\theta$. The three double singularities are labelled by the signatures of the corresponding intervals. Compare the position of these singularities with the position of the extremal angles in figures 4, 5 and 6.

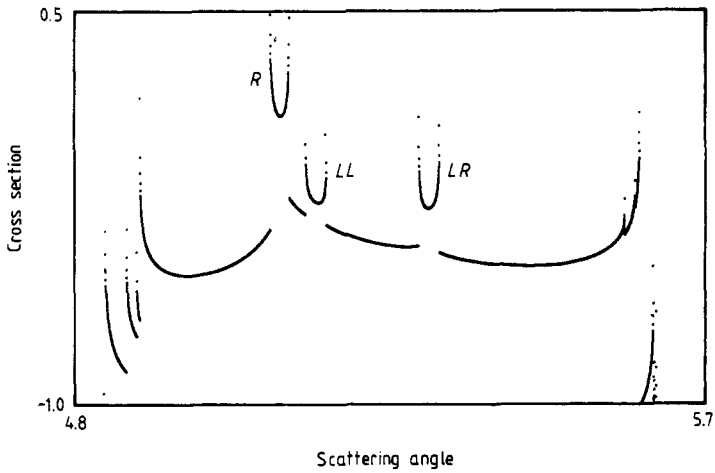


**Figure 8.** Contribution of the intervals *R*, *LL*, *LR* to the cross section. The logarithm of the cross section is plotted as a function of the scattering angle.

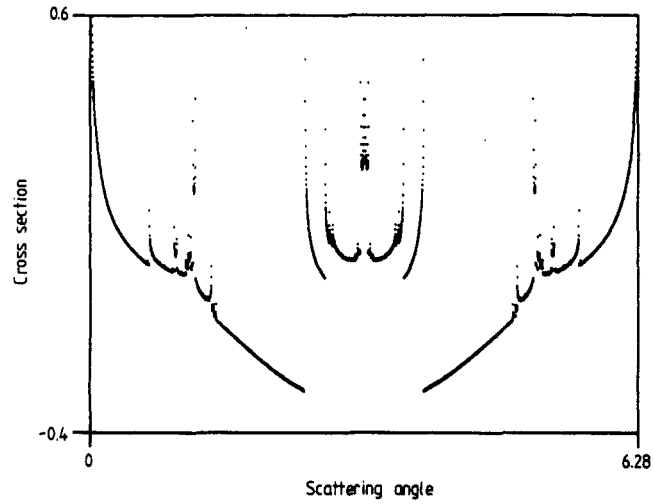


**Figure 9.** The complete differential cross section of the potential for $\alpha = \pi$ and $E = 0.6$. The logarithm of the cross section is plotted as a function of the scattering angle.

Figure 9 gives the complete cross section of the system. This plot has been produced by another method than for figures 3 and 8. In figure 9 we have started 1600 000 trajectories, evenly distributed in the impact parameter interval $(-4, 4)$. The scattering angle interval $(0, 2\pi)$ has been divided into 3600 boxes and hits of the outgoing asymptotes into the various boxes have been counted. Unfortunately, the resolution in figure 9 is not very high. Nevertheless it gives a good impression as to how the contributions from the various intervals of continuity are superimposed on the background from scattering trajectories with large impact parameters (which do not enter the potential interior). Contributions from impact parameter values close to $b=0$ create the fourfold singularity at angles $\theta$ close to $\pi$. Compare the deflection function shown in figure 1.

## 4. Fractal arrangement of rainbow singularities

So far the most prominent features of the cross section contributions of the various intervals are the rainbow singularities, especially the nearly degenerate double singularities coming from the middle parts of the impact parameter intervals. The angular position of these singularities is different for the various intervals. In this section we show that the angular arrangement of these rainbows defines a fractal set with binary organisation, reflecting the fractal structure of the hyperbolic invariant set in the phase space. To plot figure 10 we have done the following. All intervals with signature of length smaller than or equal to 10, and with trajectories going into the angle range around $5\pi/3$, were selected out. For each of these intervals the angular position of the left side of the double singularity (corresponding to point $h$ in figures 2, 3 and 7 for interval $R$) was taken as a characteristic angle and plotted on the angle axis. In the upper frame the various contributions are sorted according to the length of the signature of the corresponding interval of continuity. In the lower frame all contributions are plotted along one line. For some contributions the corresponding signature is shown. Figure 11 is a magnification of a small angular section of figure 10, and figure 12 is a further magnification.

The binary organisation of the arrangement is evident. Comparison of figures 10, 11 and 12 shows that taking half of the plot and magnifying it is equivalent to shifting the whole structure upwards one step in the signature length.

The number of intervals of continuity is countable as can be seen from the possibility to label all intervals in closed form by finite signatures. Therefore, the number of rainbow angle values is also countable. However, the set of accumulation points of these angle values forms an uncountable Cantor set.

The position of the contributions of any interval in figure 10 can be fitted qualitatively, in the limit of long signatures, by formula (9) given below. We explain it for the contributions which lie in the left half of the plot, i.e. for $\theta$ values between 5.13 and 5.17 (the right half, for $\theta$ values between 5.27 and 5.31, can be given by a mirror-image construction). First, to any interval of generation $n$ and signature $s_1 \ldots s_n$ we assign a new symbol sequence $a_1 \ldots a_{n-1}$ as follows. If $s_{n-k+1}$ is different from $s_{n-k}$, then $a_k = 1$. If $s_{n-k+1}$ is equal to $s_{n-k}$, then $a_k = 0$. The characteristic angle of the rainbow belonging to this interval is approximately given by

$$\theta = \beta + \frac{\Delta}{2} \sum_{k=1}^{n-1} (-1)^{a_k+1} \prod_{j=1}^{k-1} \nu_{a_j} \tag{9}$$

where $\beta \approx 5.145\ldots$, $\Delta \approx 0.015\ldots$, $\nu_0 = \mu^{-1/2} \approx 0.094\ldots$, $\nu_1 = \lambda^{-1/3} \approx -0.229\ldots$ (for

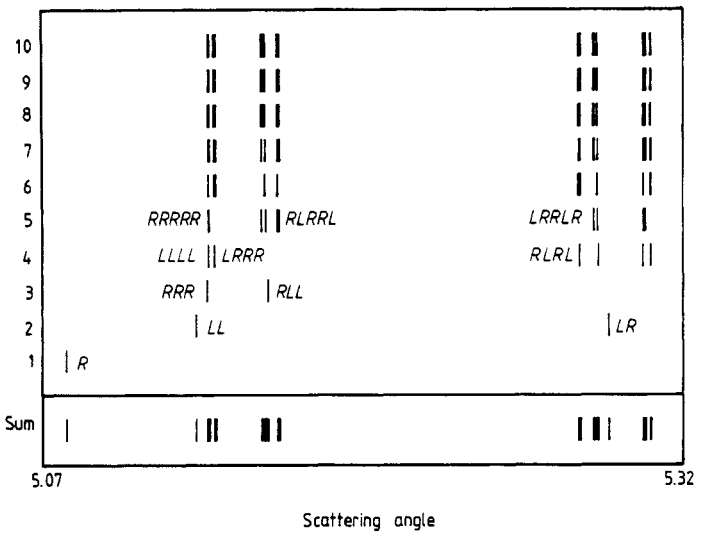


**Figure 10.** Fractal pattern of rainbow angles. In the upper frame the contributions from the various intervals are shown as a function of the signature length of the corresponding interval (vertical axis) and the angular position (horizontal axis). In the lower frame the contributions from all signature lengths are plotted on one angular axis. The signatures of some intervals are indicated.

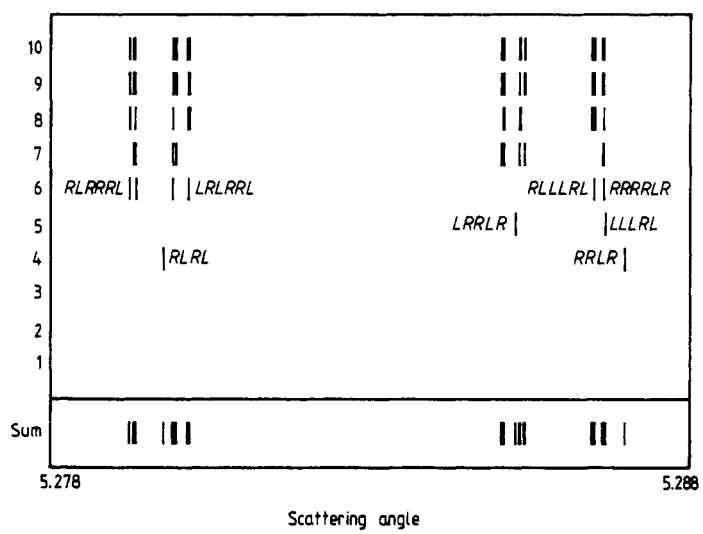


**Figure 11.** Magnification of figure 10.

the right half of the plot in figure 8 we would have to take $\beta \approx 5.29\ldots$, $\Delta \approx -0.015\ldots$). Here $\mu$ and $\lambda$ are the eigenvalues of the oscillating and the ring trajectory, respectively (compare § 3 in JS).

As the signature of intervals becomes longer and longer by accumulation of new digits in front, the corresponding position space trajectories come closer and closer to the unstable manifold of some localised orbit. In figures 4 and 7 the spirals corresponding to these intervals would converge to the spiral produced by the intersection of the asymptotic $\theta/L$ plane with this unstable manifold. In this way the fractal structure

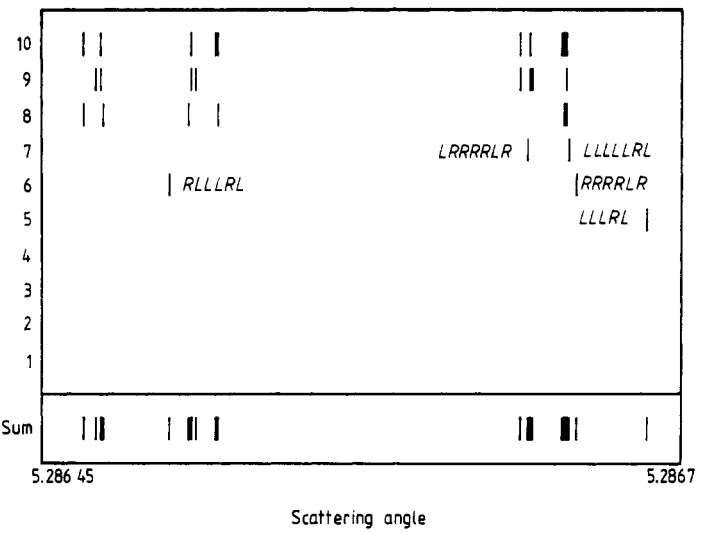


**Figure 12.** Magnification of figure 11.

seen in figure 10 is governed by the fractal structure of the bundle of unstable manifolds of the hyperbolic invariant set.

The binary organisation of this fractal set is qualitatively the same (also the scaling factors $\mu^{-1/2}$ and $\lambda^{-1/3}$ are the same) as the organisation of the set of intervals of continuity along the axis of the incoming impact parameter. This is no accident. The fractal set along the $b$ axis is given by the intersection of the stable manifolds of the localised orbits with the set of incoming asymptotes, and the stable and unstable manifolds are related via time reversal.

In figures 10, 11 and 12 we have plotted the rainbow positions around $\theta = 5\pi/3$. Since the other saddles at $\theta = \pi/3$ and $\theta = \pi$ have the same shape, we would have obtained the same plots for these other two angle ranges.

The essential features of figures 10, 11 and 12 do not depend on our choice of rainbow $h$ as a characteristic angle for each interval. Had we taken some other rainbow of interval $R$, and the corresponding rainbow of each other interval, then in the analytical fit in (9) the value of $\beta$ would be shifted and the value of $\Delta$ might be significantly smaller. Nevertheless, the succession of the contributions from the various intervals would remain exactly the same and the plots in figures 10, 11 and 12 would look qualitatively the same.

## 5. Discussion and conclusions

We have identified a fractal arrangement of rainbow singularities in the classical cross section. The plots in § 4 exhibit this structure for the particular choice of initial conditions $\alpha = \pi$ and $E = 0.6$. What happens for other values of $\alpha$ and $E$?

For other values of $\alpha$ no essential changes occur as long as the incoming stream of particles hits the stable manifolds of the hyperbolic invariant set (compare figure 9 in JS). Of course, the position of the various intervals along the $b$ axis would be shifted. However, if the signature of an interval is long enough, then the corresponding trajectories spend a long time inside the potential region and, in a sense, forget their

history. For the shape of the deflection function shown in figure 2 all that matters is how the particles leave the potential interior through one of the saddles.

When the value of $E$ is changed, eigenvalues $\mu$ and $\lambda$ of the periodic orbits are also changed (compare § 3 in JS), and the scaling properties of the fractal sets change accordingly. The difference of the values of $\varphi_+$ and $\varphi_-$ in (4) is the same for all intervals, to a very high accuracy. However, the numerical values of $\varphi_+ - \varphi_-$ depend on $E$. Accordingly the shape of the deflection function in the middle of the intervals, where the asymptotic oscillations from both sides are fitted together, depends strongly on $E$. We find an exact cubic rainbow at a critical energy $E_c \approx 0.58\ldots$. We have a cubic rainbow at angle value $\theta_c$, if there is an impact parameter value $b_c$ such that $\theta(b_c) = \theta_c$ and $(d\theta/db)(b_c) = (d^2\theta/db^2)(b_c) = 0$. At $E_c$ the two extrema $h$ and $i$ of the deflection function in figure 2 coincide. For $E < E_c$ these two extrema disappear. For $E$ increasing from $E_c$ the angular distance between these extrema increases monotonically. The fractal sets described here exist as long as $E$ lies between $E_S$ and $E_M$ (compare figure 8 in JS).

To our knowledge, such a fractal pattern of rainbow singularities in the differential cross section has not yet been described for any other scattering system. The mechanism that produces this structure depends on the existence of homoclinic or heteroclinic intersections of the invariant manifolds of localised orbits. Therefore, we expect a fractal pattern of rainbows to occur for other chaotic scattering systems too. In all such systems the boundaries of the impact parameter intervals of continuity are formed by the intersection of the $b$ axis with the stable manifolds of some localised orbits. If the initial impact parameter comes closer to a boundary point, the trajectory makes more and more revolutions along a periodic orbit, and the deflection function shows oscillations similar to those in figure 2. This leads to a corresponding sequence of rainbow singularities in the cross section. Of course, the scaling properties are given by the eigenvalues of the respective localised orbits. Because trajectories are not allowed to intersect in phase space, the images of the various intervals in the outgoing asymptotic plane corresponding to the curves shown in figures 4 and 7 must generally run in parallel, without intersections. Accordingly, the exact position of the rainbows will be slightly different for the various intervals. The accumulation locus of the various curves is given by the intersection of the $\theta/L$ plane with the unstable manifolds of the hyperbolic invariant set. Therefore, the angular distribution of the rainbows reflects the fractal arrangement of these unstable manifolds and we obtain a fractal pattern of rainbow singularities.

In this sense, the qualitative properties which we have demonstrated for our particular system should be universal for any chaotic potential scattering system. The only important difference for other systems might be that there is no such simple binary signature for the fractal sets, both for the intervals of continuity along the $b$ axis and for the rainbow distribution along the $\theta$ axis. In other cases these fractal sets might be more complicated. However, because of time reversal invariance we expect again that both of these fractal sets are arranged in essentially the same way, just reflecting the symmetry between the stable and unstable manifolds of the hyperbolic invariant set.

## Acknowledgments

We thank Professor P H Richter for helpful comments. This work has been supported financially by the Deutsche Forschungsgemeinschaft.

## References

Agmon N 1982 *J. Chem. Phys.* **76** 1309-16
Campbell D K, Peyrard M and Sodano P 1986 *Physica* **19D** 165-205
Churchill R C, Pecelli G and Rod D L 1979 *Stochastic Behaviour in Classical and Quantum Hamiltonian Systems* ed G Casati and J Ford (Berlin: Springer) pp 76-136
Eckhardt B 1988a *Europhys. Lett.* **5** 107-11
—— 1988b *Physica* **33D** 89-98
Eckhardt B and Aref H 1988 *Phil. Trans. R. Soc.* A **326** 655-96
Eckhardt B and Jung C 1986 *J. Phys. A: Math. Gen.* **19** L829-33
Fitz D E and Brumer P 1979 *J. Chem. Phys.* **70** 5527-33
Gottdiener L 1975 *Mol. Phys.* **29** 1585-95
Jung C and Scholz H-J 1987 *J. Phys. A: Math. Gen.* **20** 3607-17
—— 1988 *J. Phys. A: Math. Gen.* **21** 2301-11
Noid D W, Gray S K and Rice S A 1986 *J. Chem. Phys.* **84** 2649-52
Petit J M and Henon M 1986 *Icarus* **66** 536-55
Rankin C C and Miller W H 1971 *J. Chem. Phys.* **55** 3150-6
Schlier C G 1983 *Chem. Phys.* **77** 267-75
Skodje R T and Davis M J 1988 *J. Chem. Phys.* **88** 2429-56
Troll G and Smilansky U 1989 *Physica* **35D** 34-64